Mechanical stress by spasticity accelerates fracture healing after spinal cord injury

Sakitani, Naoyoshi

(Degree)
博士（保健学）

(Date of Degree)
2018-03-25

(Date of Publication)
2019-03-01

(Resource Type)
doctoral thesis

(Report Number)
甲第7167号

(URL)
https://hdl.handle.net/20.500.14094/D1007167

博　士　論　文

Mechanical stress by spasticity accelerates fracture healing after spinal cord injury
（脊髄損傷後の骨折は痙性麻痺の筋緊張亢進で生じたメカニカルストレスによって早く治癒する）

平成 30 年 1 月 17 日

神戸大学大学院保健学研究科保健学専攻

Sakitani Naoyoshi
崎谷直義

Contents

Abstract

Accelerated fracture healing in patients with spinal cord injuries (SCI) is often encountered in clinical practice. However, there is no distinct evidence in the accelerated fracture healing, and the mechanisms of accelerated fracture healing in SCI are poorly understood. We aimed to determine whether SCI accelerated fracture healing in morphology and strength, to characterize the healing process with SCI, and to clarify the factors responsible for accelerated fracture healing. In total, 39 male Wistar rats were randomly divided into healthy control without intervention, SCI only, fracture with SCI, botulinum toxin (BTX) A-treated fracture with SCI, and propranolol-treated fracture with SCI groups. These rats were assessed with computed microtomography, histological, histomorphological, immunohistological, and biomechanical analyses. Both computed microtomography and histological analyses revealed the acceleration of a bony union in animals with SCI. The strength of the healed fractures after SCI recovered to the same level as that of intact bones after SCI, while the healed bones were weaker than the intact bones. Immunohistology revealed that SCI fracture healing was characterized by formation of callus with predominant

intramembranous ossification and promoting endochondral ossification. The accelerated fracture healing after SCI was attenuated by BTX injection, but did not change by propranolol. We demonstrated that SCI accelerate fracture healing in both morphology and strength. The accelerated fracture healing with SCI may be due to predominant intramembranous ossification and promoting endochondral ossification. In addition, our results also suggest that muscle contraction by spasticity accelerates fracture healing after SCI.

Keywords

Spinal cord injuries, Fracture healing, Acceleration, Endochondral ossification, Intramembranous ossification, Botulinum toxin A

Introduction

Spinal cord injuries (SCI) cause paralysis of motor and sensory control at regions below the neurological lesion. Muscle atrophy [1], joint contracture [2], and bone disease [3-5] are the major complications of SCI in the sublesional area. Among SCI patients, more than 50% have developed bone disease, including bone atrophy, heterotopic ossification, and fractures [6]. In particular, fracture is a prevalent complication of SCI, and in clinical settings, the fracture associated with SCI tends to heal quickly. This phenomenon has been demonstrated by some clinical studies [5, 7]. These findings inspired us to investigate the process of fracture healing with SCI.

To our knowledge, 7 animal studies have investigated the effects of SCI on fracture healing. Three studies [8-10] have shown that fracture healing was delayed after SCI, when fractured at 2 or 3 weeks after SCI. In contrast, the remaining four studies, which examined the fracture coincided with SCI, have showed early bony bridging [11], enhanced callus formation [12], enhanced callus ossification [13, 14], and accelerated endochondral ossification [11]; then these findings indicate that SCI led to accelerated fracture healing. However, this evidence is based on the results observed in

rats from 0 to 28 days after the fracture, except one sample of 56 days after the fracture reported by Aro et al. [13]. Regardless, normal fracture healing takes 35-42 days to achieve complete healing in rats [15]. Considering the research as a whole, little is known about the process of restoration to the bone's original shape and structure from the fractures with SCI. Unfortunately, the radiographic analysis and qualitative histological evaluation used in earlier studies [13] lack the discriminative power and quantitative properties that would enable a distinct differentiation between normal and SCI fracture healing. Furthermore, the most meaningful clinical assessment of fracture healing is the return of the mechanical strength of the healed bone. However, the mechanical strength of the healed bone after SCI has not been evaluated.

An intriguing question that arises from these studies is what is contributing to the acceleration of fracture healing with SCI. Spasticity [16] and autonomic hyperreflexia [17] are a representative complication of SCI. Spasticity produces hypertonicity when the spastic muscle continuously contracts. Muscular contraction induced by electrical stimulation improves bone atrophy [18], whereas hypertonia with botulinum injections impairs fracture healing [19]. Thus, mechanical stress by muscular

contraction may have impact on fracture healing. On the other hand, autonomic hyperreflexia leads to increased sympathetic activity. Recently, there have been many reports concerning participation of sympathetic nervous system in regulating bone metabolism [20-23]. Although its physiologic mechanism remains to be elucidated at present, increased sympathetic activity unequivocally affects bone metabolism.

The objectives of this paper were to determine whether SCI result in accelerated fracture healing in bone structure and mechanical strength and to characterize the process of accelerated fracture healing with SCI. Furthermore, we assessed the contribution of the spasticity or autonomic hyperreflexia that is suspected to be the cause to accelerated fracture healing after SCI.

Materials and Methods

Experimental Design

All experimental procedures were examined by the Institutional Animal Care and Use Committee, approved by the president of Kobe University, and performed according to the Kobe University Animal Experimentation Regulations. A total of 39 male Wistar

rats (16 weeks old, 380-400 g mean body weight, Japan SLC Inc., Japan) were used for this study. Male rats aged 16 weeks were chosen to avoid the effects of estrogen [24] and rapid growth [25] to bone. Animals were housed in pairs in standard cages under a 12h dark/light cycle at a constant temperature of 22 ± 1 °C and allowed free access to standard food and water. These rats were randomly divided into a healthy control group that had no intervention (control group), non-fractured spinal cord injuries (SCI group), fracture group, and fracture with SCI (fracture + SCI group). In addition, to assess the contribution of the spasticity, botulinum toxin (BTX)-A was injected into muscles surrounding the fracture line after fracture with SCI (BTX group), and to eliminate the sympathetic overactivity effect, the β-adrenergic antagonist, propranolol, was administered intraperitoneally after fracture with SCI (propranolol group). The right and left femurs of each animal served as different samples. Total 78 femurs were assessed by synchrotron radiation computed microtomography (SR-μCT), μCT, histological analysis, histomorphometric analysis, immunohistochemical analysis, and mechanical testing. For SR-μCT, histological analysis, histomorphometric analysis, and immunohistochemical analysis, we compared the fracture + SCI group with the fracture

group at 7, 14, 28, and 49 days after fracture (n = 6 limbs at each time point). The BTX and propranolol groups were assessed with μCT and histological analysis at 14 and 28 days after fracture. For mechanical testing, in addition to, the control, SCI, fracture, and fracture + SCI groups at 49 days were used (n = 4 femurs in all of the groups). The study design including the assignment of animals to respective groups is shown in supplemental Fig. 1. The sample sizes were calculated by a power analysis with a level of 0.80 based on pilot results.

Animal Model

Spinal Cord-Injured Model

The SCI surgeries conformed to the protocols in our previous studies [26-30] with a slight modification. The animals were anesthetized with pentobarbital sodium (40 mg/ kg, intraperitoneally) and buprenorphine [0.02 mg/kg, subcutaneously (s.c.)]. A midline incision was made through the skin in the distal thoracic area. The lateral paraspinal muscles were dissected along either side of the spinous processes, and the dorsal surface of vertebras from T7 to T11 was exposed. The spinal cord, which was completely transected at the level, was exposed by a laminectomy of the vertebras from T7 to T8.

Finally, the muscle and the skin were closed separately with silk sutures.

Closed Mid-Shaft Femoral Fracture Model

After SCI, the closed mid-shaft femoral fracture was produced in the bilateral femurs of the rat in fracture, fracture + SCI, BTX, and propranolol groups using the protocols of Bonnarens and Einhorn [31]. The skin over the knee joint was incised longitudinally. The patella was dislocated on the lateral side, and the articular surface of the femoral condyle was exposed. A Kirschner wire (k-wire) was inserted into the femoral canal from the intercondylar notch as an intramedullary nailing fixation. The k-wire was cut, and the patella dislocation was reduced. The joint capsule and the skin were closed. Afterward, the closed mid-shaft femoral fracture was created with a 3-point bending apparatus composed of a blunt guillotine driven by a dropped weight.

Pharmaceutical Intervention

For the BTX group, 1 UI/ml solution of BTX-A was prepared by dissolving BTX-A in 0.9% saline solution. BTX-A solution was injected into both femoral regions (quadriceps, biceps, and adductor magnus) of rats in BTX group after fracture. This dose of BTX-A per muscle has previously been shown to produce muscle relaxant for

28 days [32].

To reduce sympathetic overactivities in SCI rats, the rats of propranolol group were received a single daily intraperitoneal injections of propranolol (20 mg/kg/day) between 8:00 and 9:00 P.M. Dose and treatment protocol were based upon those described by Kondo and Togari [33] and Minkowitz et al. [34]. These methods have proven for inhibition of sympathetic activity with cardiac function analysis [35].

Postoperative Care

An analgesic (buprenorphine, 0.02 mg/kg, s.c.) was administered twice daily for 3 days after the surgery. Postoperatively, the bladders of SCI rats were manually compressed three times daily for 2 weeks and then twice daily until each time point.

Sampling

All rats were killed by exsanguination under anesthesia and analgesia at each time point. The femurs were harvested and the muscle tissues were removed from the bone. Then, we measured the callus dimensions in the anteroposterior and lateral dimensions at the fracture line using an electronic caliper (CD-S20C, Mitutoyo, Japan), and the overall callus size was the mean of these two dimensions. After measuring the callus

size, the femurs were immediately frozen and stored at -80 °C until analyzed.

μCT

We used a high-resolution computed tomography (CT) system installed in the beamline 20B2 of the synchrotron radiation facility Spring-8 (Harima, Japan). The femur of rats in the fracture and fracture + SCI groups was mounted on a stack of the computer-controlled precision stage. The photon flux transmitted through the sample was detected by a high-resolution detector consisting of a beam monitor (AA60, Hamamatsu Photonics, Hamamatsu, Japan) and a cooled charge-coupled device camera (ORCA-flash 4.0, Hamamatsu Photonics, Hamamatsu, Japan) at 25 keV. The samples were scanned with 8.03 μm voxel size. The region of interest was defined as the fractured line on the center and the upper and lower 15 mm. The femur of rats in the BTX and propranolol groups was imaged using μCT (R_mCT2, Rigaku, Tokyo, Japan). The samples were scanned with 20 μm voxel size. The region of interest was defined as the fractured line on the center and the upper and lower 10 mm. Three-dimensional reconstructions of the images were visualized with ImageJ 1.38 (ImageJ, NIH, USA). To distinguish mineralized and non-mineralized tissues, the thresholding values were set

at 641.9 mg HA/cm^3.

Histology

Tissue Preparation for Histology

We prepared undecalcified frozen sections as previously described in the literature [36]. The bones were embedded in super cryoembedding medium (SCEM, Section-lab, Japan). Each sample was sectioned at a thickness of 5 μm with a disposable tungsten carbide blade at a central point in the bone (5 sections per a sample). Four samples from each group were used for histological, histomorphometric, or immunohistochemical analyses.

Histological and Histomorphometric Analyses

Frozen sections were stained with safranin-O-fast green. They were captured with a light microscope (BX-53, Olympus, Japan) at a magnification of ×4. The degree of fracture healing was evaluated using the 5-point scale following the method described by Allen et al. [37]. The histomorphometric parameter was measured as described by Colnot [38]. Briefly, the areas of fibrous tissue, cartilage tissue, and newly formed bone tissue were assessed as a percentage of the total callus area with Adobe Photoshop CS

(Adobe Systems Inc., Japan).

Immunohistochemical Analysis

The frozen sections were incubated with mouse monoclonal anti-collagen Type I (diluted 1: 4000, C2456, Sigma-Aldrich, USA), mouse monoclonal anti-collagen Type II (diluted 1: 1000, F57, Daiichi Fine Chemical, Japan), rabbit polyclonal anti-collagen Type X (diluted 1: 1000, LB-0092, LSL, Japan), or mouse monoclonal anti-CD68 (diluted 1: 2000, MCA341GA, Serotec, UK) antibodies. A subsequent reaction was made using the strep-tavidin-biotin-peroxidase complex technique with an Elite ABC kit (diluted 1: 50, PK-610, Vector Laboratories, USA). Then, the 3,30-diaminobenzidine tetrahydrochloride (K3466, Dako Japan, Japan) was used for the visualization of the immunoreaction. The sections were finally counterstained with hematoxylin, washed in water, and coverslipped. They were captured with a light microscope (BX-53, Olympus, Japan) at a magnification of ×4. Type I, II, and X collagen-positive areas were measured as a percentage of total callus area with Adobe Photoshop CS (Adobe Systems Inc., Japan).

Mechanical Testing

The k-wire was removed, and the femurs were thawed to room temperature for 2 h. The functional mechanical properties of the bone were then assessed by a 3-point bending test with a load torsion and bending tester (AUTOGRAPH, Shimazu, Japan). The sample was placed on supports located at a distance of 20 mm. The bending force was applied midway between the supports on the anterior surface at a speed of 2 mm/min until the fracture occurred. During the mechanical testing, load-deflection data were recorded. The load-deflection curve provided the biomechanical parameters as follows: ultimate loads at failure (the maximum force endured by femur), stiffness (the slope of the linear portion of the curve), and energy-to-failure (the area under the curve).

Statistical Analysis

The results of the callus size, histomorphometric analysis, and mechanical testing are presented as the mean ± standard deviation (SD), and the degree of fracture healing is presented as the median (25-75%). All statistical analyses were performed using SPSS 22 for Mac (SPSS Japan, Japan). A Student's t test was used to compare the callus size or histomorphometric analysis between the fracture and fracture + SCI groups at each time point. A one-way ANOVA assessed the differences between all groups for

mechanical testing with a Tukey's test. The Mann-Whitney U test was applied to compare the degree of fracture healing between the fracture and fracture + SCI groups at each time point. An alpha value less than 0.05 was chosen as the significance level for these statistical analyses.

Results

General Observations

All of the rats survived throughout the experimental period, were active, and appeared healthy except for hindlimb functional deficits associated with SCI such as the motor paralysis and sensory paralysis. The body weight of the fracture + SCI rats tended to be lower than that of fracture rats at all time points (325.0 ± 30.6 vs. 354.3 ± 14.7 g at 7 days; 295.3 ± 44.1 vs. 381.3 ± 3.1 g at 14 days; 356.3 ± 6.1 vs. 375.0 ± 22.2 g at 28 days; 369.6 ± 20.1 vs. 442.6 ± 23.1 g at 49 days); however, fracture + SCI rats gained weight after 14 days, indicating general good health.

The response to stimuli disappeared, and rats of SCI, fracture + SCI, BTX, and propranolol groups demonstrated complete flaccid paraplegia during the first few

days after the injury, and thereafter showed kick movements, clonic and high-frequency flexion-extension movements, and hyperreflexive response which were defined as spasticity [39]. The rats in BTX group showed the reflex response to stimuli, but the kick movements were not observed. These results indicated that the dose of BTX in our study was adequate to inhibit spasticity after SCI.

μCT

Representative 3D images in each group are presented in Fig. 1. At 7 and 14 days, the fracture gap was observed in the fracture and fracture + SCI groups. At 28 days, the fracture + SCI group exhibited bony bridging of the fractured bone ends, while the fracture group did not exhibit bony bridging. At 49 days, the cortices had completely bridged in both the groups. On the other hand, the fracture gap in both BTX and propranolol groups was clearly observed at 14 days, and then the bony union was observed in both the groups at 28 days.

Callus Size

The callus size measurements indicated significant differences between the fracture and fracture + SCI groups at all the time points (7.91 ± 0.82 vs. 4.93 ± 0.37 mm at 7 days;

7.91 ± 0.82 vs. 6.50 ± 0.63 mm at 14 days; 7.90 ± 0.48 vs. 5.73 ± 0.69 mm at 28 days; 6.14 ± 0.89 vs. 4.92 ± 0.57 mm at 49 days; $p < 0.05$) (Fig. 2). These results indicated that the fractured bone of SCI rats formed a smaller callus than that of the fractured rats at all of the time points.

Fracture Healing Score

The median value of fracture healing scores at 7 days was significantly lower in the fracture + SCI group than in the fracture group [fracture + SCI, 0 (0–0) vs. fracture, 1 (1–1), $p < 0.05$]. However, at 14 days the fracture healing score revealed the same degree of fracture healing [fracture + SCI, 1 (1–1) vs. fracture, 1 (1–1.25), n.s.]. At 28 days, the degree of fracture healing was significantly higher in the fracture + SCI group than that in the fracture group (fracture + SCI, 4 (4–4) vs. fracture, 3.5 (3–4), $p < 0.05$). Moreover, no significant differences were found between the groups at 49 days [fracture + SCI, 4 (4–4) vs. fracture, 4 (4–4), n.s.].

Histology and Histomorphometry

At 7 days after the fracture, cartilage tissue was undetected and slight woven bone was formed beneath the periosteum at the fracture site in the fracture + SCI group, whereas

woven bone and cartilage tissue were observed at the fracture region in the fracture group. At 7 days after fracture, the cartilage area in the fracture + SCI group was significantly smaller than that in the fracture group ($p < 0.05$) (Fig. 3b). At 14 days, woven bone and cartilage tissue were observed, bony bridging was undetected at the fracture area, and the fracture gaps still existed in fracture and fracture + SCI groups. At 28 days, the fracture + SCI group exhibited a bony bridge that consisted of cortical bone and slight woven bone. On the other hand, the fracture group had a bony bridge that consisted of woven bone. At 49 days, cortical bone bridged the fracture gap in the fracture + SCI group, while cortical bridging occurred with slight woven bone in the fracture group.

The morphology of fracture healing callus was not different in fracture + SCI rats with or without BTX at 14 days. At 28 days, the fracture + SCI group exhibited a bony bridge that consisted of cortical bone and slight woven bone; however, the BTX group had a bony bridge that consisted of woven bone (Fig. 4). The propranolol treatment did not affect the histology of fracture healing after SCI at 14 and 28 days (Fig. 4).

Immunohistochemistry

At 7 days, only type I collagen immunostaining was detected [4 out of 4 samples were positive. The positive area was 15.0 ± 6.3%. The area was smaller than that of fracture group ($p < 0.01$)], but neither type II [2 out of 4 samples were negative. The positive area was 1.1 ± 1.6%. The area of fracture + SCI group was smaller than that of fracture group ($p < 0.01$)] nor type X collagen [4 out of 4 samples were negative. The positive area was 0 ± 0%. The area of fracture + SCI group was smaller than that of fracture group ($p < 0.05$)] immunostaining was observed in the fracture callus of the fracture + SCI rats. The immunohistochemical detection of type II and type X collagen provides a molecular marker distinguishing between bone formed by intramembranous and endochondral ossification. These results indicated that the newly formed bone in the fracture + SCI group at 7 days was intramembranous bone. On the other hand, we observed immunoreactivity to type I collagen (4 out of 4 samples were positive. The positive area was 73.2 ± 9.6%.), type II collagen (4 out of 4 samples were positive. The positive area was 17.5 ± 3.3%.), and X collagen (4 out of 4 samples were positive. The positive area was 3.1 ± 1.5%.) found in the fracture callus of the fractured rats. The

results indicated that the newly formed bone in the fracture group was both intramembranous and endochondral bone. At 14 days, the immunoreactivity to type I collagen (fracture + SCI group, 4 out of 4 samples were positive. The positive area was 25.9 ± 13.5%; fracture group, 4 out of 4 samples were positive. The positive area was 27.9 ± 22.3%. No significant difference was found between groups.), type II collagen (fracture + SCI group, 4 out of 4 samples were positive. The positive area was 20.4 ± 6.2%; fracture + SCI group, 4 out of 4 samples were positive. The positive area was 43.9 ± 20.7%. No significant difference was found between groups.), and type X collagen (fracture + SCI group, 4 out of 4 samples were positive. The positive area was 5.7 ± 3.2%; fracture group, 4 out of 4 samples were positive. The positive area was 11.5 ± 7.6%. No significant difference was found between groups.) was observed in the callus of the fracture and fracture + SCI groups. These results indicated that both the intramembranous and endochondral ossification occurred in both the fracture and fracture + SCI groups (Fig. 5).

Positive immunolabeling for CD68 was observed in the fractured callus of the fracture and fracture + SCI rats at 7 days. The degree of immunoreactivity in the callus

of the fracture + SCI rats was lower than that of the fractured rats. At 14, 28, and 49 days, both the groups exhibited the same level of immunoreactivity for CD68 at the surface of the newly formed bone (Fig. 6).

Mechanical Testing

The ultimate loads at failure in the control, fracture, SCI, and fracture + SCI groups were 152.00 ± 17.62, 140.84 ± 60.13, 90.00 ± 22.05, and 105.58 ± 7.12 N, respectively. The bone strength in the fracture group recovered to the same level as that of the control group. Similarly, the bone strength of the fracture + SCI group returned to the same level as that of the SCI group. However, the bone strength of the SCI and fracture + SCI groups was significantly lower than that of the control group ($p < 0.05$), and this result showed that the bones of the SCI and fracture + SCI groups were weak in comparison to that of the control group. The stiffness in the control, fracture, SCI, and fracture + SCI groups were 249.88 ± 59.96, 114.96 ± 32.62, 205.77 ± 15.67, and 88.94 ± 15.73 N/m, respectively. The stiffness in the fracture group was significantly lower than that in the control and SCI groups ($p < 0.05$). The stiffness in the fracture + SCI group was significantly lower than that in the SCI group ($p < 0.01$). The energy-to-failure in the

control, fracture, SCI, and fracture + SCI groups were 320.46 ± 35.35, 239.10 ± 12.59, 110.71 ± 14.83, and 121.11 ± 31.12 mJ, respectively. The energy-to-failure in the fracture group returned to the same level as that in the control group. The energy-to-failure in the fracture + SCI group returned to the same level as that of the SCI group. However, the energy-to-failure in the fracture + SCI group and SCI groups was significantly lower than that in the control group ($p < 0.01$).

Discussion

The aims of this study were to determine whether fractures with SCI heal earlier in terms of their morphological and mechanical properties than normal fractures, to characterize the process of accelerated fracture healing with SCI, and to clarify the factors responsible for accelerated fracture healing. Similar to a previous studies of humans [5, 7] and animals [11, 13, 14], in the present study the acceleration of fracture healing with SCI was confirmed. This is because the SCI fractures exhibited a rapid and full recovery of bone morphology and the same degree of functional recovery of the bones after SCI. Eventually, we found that SCI fractures led to an approximately 40%

decrease in the time for the synchrotron radiographic healing of femoral fractures, in which the SCI fractures healed in 28 days, rather than the 49 days in the fracture group. We also found that the fracture after SCI in the early phase predominantly healed through intramembranous ossification, whereas that of the normal fractures through both intramembranous and endochondral ossifications. In addition, the time required for the completion of endochondral ossification in SCI fracture was shorter than that in normal fracture. Therefore, the accelerated fracture healing with SCI may be due to predominant intramembranous ossification and promoting endochondral ossification. Furthermore, the present findings may shed light on what's underlying this phenomenon and provide evidence that muscle contraction by spasticity contributes to the acceleration of fracture healing after SCI. The accelerated fracture healing was attenuated in SCI fracture treated with BTX, and therefore this result indicates that mechanical stress by spasticity has significant roles in accelerated fracture healing with SCI.

We have demonstrated that the morphological recovery of a fractured bone in the fracture + SCI rats was faster than that in the fracture rats. The SR-μCT analysis

showed that the bony bridging of the fracture gap occurred earlier in the fracture + SCI rats than in the fracture rats. μCT is a more sensitive tool for detecting changes that occur during fracture healing than X-rays that were used in the previous studies. In addition, SR-μCT provides superior resolution to μCT. Thus, we could evaluate the morphological differences in the healing process in greater detail. These date are consistent with histologic and histomorphometric analyses, which revealed that the cortical bridging fracture union was more rapid in the fracture + SCI rats than in the fractured rats. The newly formed bone after the fracture recovers generally the original bony shape and strength through remodeling immature woven bone into mature cortical bone. The fracture healing score of fractures with SCI exhibited a significantly higher score at 28 days. Collectively, these results demonstrated that SCI accelerated the recovery of the bone morphology after the fracture.

Our mechanical testing indicates that the strength and energy-to-failure of healed bone with SCI returned to the same level as that of non-fractured bone with SCI. Nonetheless, the healed bone with SCI was more fragile than the healthy control bone. The loss of bone strength induced by bone loss after SCI has been well documented in

animal studies [40-43]. Therefore, the weakness of SCI fractures may be attributed to bone atrophy after SCI.

Fractured bone commonly heals through the following stages: (1) inflammation; (2) callus formation; and (3) remodeling. In the inflammatory stage, inflammatory cells such as macrophages ingest necrotic tissue after the fracture. The newly formed bone was formed by endochondral ossification and intramembranous ossification, and endochondral ossification predominates in the callus formation stage. In the remodeling stage, the newly formed bone is remodeled into the pre-fractured bone shape. According to histomorphometry and immunohistochemistry for type I, II, and X collagen, both the intramembranous and endochondral ossification occurred in the fracture group. However, SCI fractures exhibited only intramembranous ossification in the callus at 7 days corresponding to the stage of inflammation or callus formation. At 14 days, the intramembranous and endochondral ossification occurred in the fracture and fracture + SCI groups. However, the endochondral ossification phase in SCI fracture was shorter than that in normal fracture, because the start of endochondral ossification in SCI fracture was late. In addition, these changes might be reflected in a

decrease in the callus size in the fracture + SCI rats. Taken together, SCI fracture healing was characterized by the formation of callus with predominant intramembranous ossification and promoting endochondral ossification. The characteristic callus formation after SCI may contribute to accelerated fracture healing. Intramembranous ossification does not involve formation of intermediate cartilaginous tissue, while endochondral ossification involves formation and subsequent remodeling of cartilage to bone tissue. The formation and subsequent remodeling of cartilage to bone tissue requires long time. Therefore, the change of ossification pattern from endochondral ossification to intramembranous ossification can lead to rapid bone formation, and thus the bony union of fracture site could be achieved early. The stability of the fracture fixation affects the ossification pattern in healing fracture [44]. We used intramedullary nailing developed by Einhorn et al. [31] as the fixation of fracture. The fixation method has some limitations with regards to fracture stability; unlocked intramedullary rod does not provide a resistance to torsional and weight bearing. Therefore, SCI-induced non-weight loading may affect the change of ossification pattern. However, Aro et al. [13]. contributed to this possibility using hip dislocation-

induced non-weight loading model. The change of fracture healing process associated with SCI is not simply due to a reduction in weight loading as postulated by Aro et al.. Additionally, the immunohistology analysis in the fracture callus of the fracture + SCI rats revealed fewer macrophages at 7 days after the fracture. Macrophages have been associated with cartilage formation, and a decrease in macrophage-impaired cartilage maturation [45]. Therefore, the change in ossification may result from a decrease in the number of macrophages.

The present study attempted to verify the hypothesis that spasticity and/or sympathetic overactivity contribute to accelerated fracture healing in SCI rats. Consequently, the accelerated fracture healing after SCI was canceled out by BTX injection, but did not change by propranolol. The intramuscular administration of BTX attenuates a spastic muscle's ability to generate mechanical stress by muscle contraction. The present results suggest that increased muscle contraction caused by spasticity accelerated fracture healing after SCI. A recent report disclosed that muscle contraction elicited by electrical stimulation protects against SCI-related bone loss, and that muscle contraction can increase mechanical stress on bone and lead to increased

bone volume [18]. Additionally, the importance of muscle-derived mechanical stress for bone healing was confirmed by the work of Hao et al. [19] that evaluated the effect of muscle paralysis on normal femoral fracture healing. Paralysis of quadriceps muscle by administration of BTX negatively impacted the healing capacity of femoral fractures in rats. Our findings not only provide new insights into fracture healing process after SCI, but also raise intriguing possibilities for the use of muscle contraction to accelerate fracture healing.

Although novel therapies for fracture healing are constantly explored, effective therapeutic approaches have not been established in clinical settings. Our findings indicate that the acceleration of fracture healing in rats with SCI ultimately leads to new therapeutic strategies that accelerate fracture healing. However, a potential weakness of our results is that the strength of the healed bone with SCI did not return to the same level as control bones.

In conclusion, we found that the fracture with SCI healed earlier than a normal fracture in terms of both morphology and strength. Furthermore, our results indicate that accelerated fracture healing with SCI was due to predominant

intramembranous ossification and promoting endochondral ossification. Our results also suggest that the muscle contraction by spasticity is an important factor responsible for accelerated fracture healing after SCI.

Acknowledgements

We would like to thank Daichi Watanabe and Kousuke Watanabe for animal care. We are also grateful to Daisuke Inoue, Akira Ito, and Hiroki Iijima for their support with mechanical testing. The synchrotron radiation experiments were performed at the BL20B2 of Spring-8 with the approval of the Japan Synchrotron Radiation Research Institute (JASRI) (Proposal No. 2014A1681). This study was supported by Grant-in-Aid for Challenging Exploratory Research (25560260) from the Japan Society for the Promotion of Science (JSPS).

Author Contributions

Conception and design on the study: HM. Acquisition of the data: NS, HI, and MN. Analysis and interpretation of the data: NS, YM, JO, and HM. Drafting the article: NS,

HK, JO, and HM. Technical support: YM, HK, and JO. Critical revision of the article for important intellectual content: NS, HI, MN, YM, HK, JO, and HM. All authors read and approved the final manuscript.

Compliance with Ethical Standards

Conflict of interest

Naoyoshi Sakitani, Hiroyuki Iwasawa, Masato Nomura, Yasushi Miura, Hiroshi Kuroki, Junya Ozawa and Hideki Moriyama certifies that he or a member of his immediate family, has no commercial associations (e.g., consultancies, stock ownership, equity interest, patent/licensing arrangements, etc.) that might pose a conflict of interest in connection with submitted article.

Human and Animal Rights and Informed Consent

All applicable international, national, and/or institutional guidelines for the care and use of animal were followed. All procedures performed in studies involving animals were in accordance with the ethical standards of the institution or practice at which the studies were conducted. This article does not contain any studies with human participants

performed by any of the authors.

References

1. Giangregorio L, McCartney N (2006) Bone loss and muscle atrophy in spinal cord injury: epidemiology, fracture prediction, and rehabilitation strategies. J Spinal Cord Med 29:489-500. doi:10.1080/10790268.2006.11753898

2. Harvey LA, Herbert RD (2002) Muscle stretching for treatment and prevention of contracture in people with spinal cord injury. Spinal Cord 40:1-9. doi:10.1038/sj.sc.3101241

3. Ranganathan K, Loder S, Agarwal S, Wong VW, Forsberg J, Davis TA, Wang S, James AW, Levi B (2015) Heterotopic ossification: basic-science principles and clinical correlates. J Bone Joint Surg Am 97:1101-1111. doi:10.2106/JBJS.N.01056

4. Jiang SD, Dai LY, Jiang LS (2006) Osteoporosis after spinal cord injury. Osteoporos Int 17:180-192. doi:10.1007/s00198-005-2028-8

5. Wang L, Yao X, Xiao L, Tang X, Ding H, Zhang H, Yuan J (2014) The effects of

spinal cord injury on bone healing in patients with femoral fractures. J Spinal Cord Med 37:414-419. doi:10.1179/2045772313Y.0000000155

6. Gifre L, Vidal J, Carrasco JL, Filella X, Ruiz-Gaspa S, Muxi A, Portell E, Monegai A, Guanabens N, Peris P (2015) Effect of recent spinal cord injury on wnt signaling antagonists (Sclerostin and Dkk-1) and their relationship with bone loss. A 12-month prospective study. J Bone Miner Res 30:1014-1021. doi:10.1002/jbmr.2423
7. Ragnarsson KT, Sell GH (1981) Lower extremity fractures after spinal cord injury: a retrospective study. Arch Phys Med Rehabil 62:418-423
8. Ding WG, Liu JB, Wei ZX (2012) Spinal cord injury causes more damage to fracture healing of later phase than ovariectomy in young mice. Connect Tissue Res 53:142-148. doi:10.3109/03008207.2011.614365
9. Ding WG, Jiang SD, Zhang YH, Jiang LS, Dai LY (2011) Bone loss and impaired fracture healing in spinal cord injured mice. Osteoporos Int 22:507-515. doi:10.1007/s00198-010-1256-8
10. Medalha CC, Santos AL, Veronez Sde O, Fernandes KR, Magri AM, Renno AC

(2016) Low level laser therapy accelerates bone healing in spinal cord injured rats. J Photochem Photobiol, B 159:179-185. doi:10.1016/j.jphotobiol.2016.03.041

11. Miyamoto T (1987) An experimental study on fracture healing in paraplegic rats. Nihon Seikeigeka Gakkai Zasshi 61:1135-1145

12. Wang L, Tang X, Zhang H, Yuan J, Ding H, Wei Y (2011) Elevated leptin expression in rat model of traumatic spinal cord injury and femoral fracture. J Spinal Cord Med 34:501-509. doi:10.1179/2045772311Y.0000000034

13. Aro H, Eerola E, Aho AJ, Penttinen R (1981) Healing of experimental fractures in the denervated limbs of the rat. Clin Orthop Relat Res. doi:10.1097/00003086-198103000-00034

14. Aro H, Eerola E, Aho AJ (1985) Fracture healing in paraplegic rats. Acta Orthop Scand 56:228-232

15. Histing T, Garcia P, Holstein JH, Klein M, Matthys R, Nuetzi R, Steck R, Laschke MW, Wehner T, Bindl R, Recknagei S, Stuermer EK, Vollmar B, Wildemann B, Lienau J, Willie B, Peters A, Ignatius A, Pohlemann T, Claes L,

Menger MD (2011) Small animal bone healing models: standards, tips, and pitfalls results of a consensus meeting. Bone 49:591-599. doi:10.1016/j.bone.2011.07.007

16. Khurana SR, Garg DS (2014) Spasticity and the use of intrathecal baclofen in patients with spinal cord injury. Phys Med Rehabil Clin N Am 25:655-669. doi:10.1016/j.pmr.2014.04.008

17. Partida E, Mironets E, Hou S, Tom VJ (2016) Cardiovascular dysfunction following spinal cord injury. Neural Regen Res 11:189-194. doi:10.4103/1673-5374.177707

18. QinW,SunL,CaoJ,PengY,WuY,CreaseyG,LiJ,QinY,Jarvis J, Beuman WA, Zaidi M, Cardozo C (2013) The central nervous system (CNS)-independent anti-bone-resorptive activity of muscle contraction and the underlying molecular and cellular signatures. J Biol Chem 288:13511-13521. doi:10.1074/jbc.M113.454892

19. Hao Y, Ma Y, Wang X, Jin F, Ge S (2012) Short-term muscle atrophy caused by botulinum toxin-A local injection impairs fracture healing in the rat femur. J

Orthop Res 30:574-580. doi:10.1002/jor.21553

20. Takeda S, Karsenty G (2008) Molecular bases of the sympathetic regulation of bone mass. Bone 42:837-840. doi:10.1016/j.bone.2008.01.005

21. Driessler F, Baldock PA (2010) Hypothalamic regulation of bone. J Mol Endocrinol 45:175-181. doi:10.1677/JME-10-0015

22. He JY, Jiang LS, Dai LY (2011) The roles of the sympathetic nervous system in osteoporotic diseases: a review of experimental and clinical studies. Ageing Res Rev 10:253-263. doi:10.1016/j.arr.2011.01.002

23. Fonseca TL, Jorgetti V, Costa CC, Capelo LP, Covarrubias AE, Moulatlet AC, Teixeira MB, Hesse E, Morethson P, Beber EH, Freitas FR, Wang CC, Nonaka KO, Oliveira R, Casarini DE, Zorn TM, Brum PC, Gouveia CH (2011) Double disruption of α2A- and α2C-adrenoceptors results in sympathetic hyperactivity and high-bone-mass phenotype. J Bone Miner Res 26:591-603. doi:10.1002/jbmr.243

24. McCann RM, Colleary G, Geddis C, Clarke GR, Jordan GR, Dickson GR, Marsh D (2008) Effect of osteoporosis on bone mineral density and fracture

repair in a rat femoral fracture model. J Orthop Res 26:384-393. doi:10.1002/jor.20505

25. Kilborn SH, Trudel G, Uhthoff H (2002) Review of growth plate closure compared with age at sexual maturity and lifespan in laboratory animals. Contemp Top Lab Anim Sci 41:21-26

26. Moriyama H, Yoshimura O, Sunahori H, Nitta H, Imakita H, Saka Y, Maejima H, Tobimatsu Y (2004) Progression and direction of contractures of knee joints following spinal cord injury in the rat. Tohoku J Exp Med 204:37-44. doi:10.1620/tjem.204.37

27. Moriyama H, Yoshimura O, Kawamata S, Takayanagi K, Kurose T, Kubota A, Hosoda M, Tobimatsu Y (2008) Alteration in articular cartilage of rat knee joints after spinal cord injury. Osteoarthr Cartil 16:392-398. doi:10.1016/j.joca.2007.07.002

28. Moriyama H, Yoshimura O, Kawamata S, Takemoto H, Saka Y, Tobimatsu Y (2007) Alteration of knee joint connective tissues during contracture formation in spastic rats after an experimentally induced spinal cord injury. Connect Tissue

Res 48:180-187. doi:10.1080/03008200701413512

29. Moriyama H, Tobimatsu Y, Ozawa J, Kito N, Tanaka R (2013) Amount of torque and duration of stretching affects correction of knee contracture in a rat model of spinal cord injury. Clin Orthop Relat Res 471:3626-3636. doi:10.1007/s11999-013-3196-z

30. Iwasawa H, Nomura M, Sakitani N, Watanabe K, Watanabe D, Moriyama H (2016) Stretching after heat but not after cold decreases contractures after spinal cord injury in rats. Clin Orthop Relat Res 474:2692-2701. doi:10.1007/s11999-016-5030-x

31. Bonnarens F, Einhorn T (1984) Production of a standard closed fracture in laboratory animal bone. J Orthop Res 2:97-101. doi:10.1002/jor.1100020115

32. Pickett A, O'Keeffe R, Judge A, Dodd S (2008) The in vivo rat muscle force model is a reliable and clinically relevant test of consistency among botulinum toxin preparations. Toxicon 52:455-464. doi:10.1016/j.toxicon.2008.06.021

33. Kondo A, Togari A (2003) In vivo stimulation of sympathetic nervous system modulates osteoblastic activity in mouse calvaria. Am J Physiol Endocrinol

Metab 285:E661-E667. doi:10.1152/ajpendo.00026.2003

34. Minkowitz B, Boskey AL, Lane JM, Peariman HS, Vigorita VJ (1991) Effects of propranolol on bone metabolism in the rat. J Orthop Res 9:869-875. doi:10.1002/jor.1100090613

35. Bonnet N, Benhamou CL, Malaval L, Goncalves C, Vico L, Eder V, Pichon C, Courteix D (2008) Low dose beta-blocker prevents ovariectomy-induced bone loss in rats without affecting heart functions. J Cell Physiol 217:819-827. doi:10.1002/jcp.21564

36. Kawamoto T (2003) Use of a new adhesive film for the preparation of multi-purpose fresh-frozen sections from hard tissues, whole-animals, insects and plants. Arch Histol Cytol 66:123-143. doi:10.1679/aohc.66.123

37. Allen HL, Wase A, Bear WT (1980) Indomethacin and aspirin: effect of nonsteroidal anti-inflammatory agents on the rate of fracture repair in the rat. Acta Orthop Scand 51:595-600. doi:10.3109/17453678008990848

38. Colnot C, Thompson Z Miclau T, Werb Z, Heims JA (2003) Altered fracture repair in the absence of MMP9. Development 130:4123-4133.

doi:10.1242/dev.00559

39. Van de Meent H, Hamers FP, Lankhorst AJ, Bulse MP, Joosten EA, Gispen WH (1996) New assessment techniques for evaluation of posttramatic spinal cord function in the rat. J Neurotrauma 13:741-754. doi:10.1089/neu.1996.13.741

40. Jiang SD, Jiang LS, Dai LY(2007) Changes in bone mass, bone structure, bone biomechanical properties, and bone metabolism after spinal cord injury: a 6-month longitudinal study in growing rats. Calcif Tissue Int 80:167-175. doi:10.1007/s00223-00600085-4

41. Voor MJ, Brown EH, Xu Q, Waddell SW, Burden RL Jr, Burke DA, Magnuson DS (2012) Bone loss following spinal cord injury in a rat model. J Neurotrauma 29:1676-1682. doi:10.1089/neu.2011.2037

42. Ding WG, Yan WH, Wei ZX, Liu JB (2012) Difference in intraosseous blood vessel volume and number in osteoporotic model mice induced by spinal cord injury and sciatic nerve resection. J Bone Miner Metab 30:400-407. doi:10.1007/s00774-011-0238-y

43. Jiang SD, Jiang LS, Dai LY (2006) Spinal cord injury causes more damage to

bone mass, bone structure, biomechanical properties and bone mass, bone structure, biomechanical properties and bone metabolism than sciatic neurectomy in young rats. Osteoporos Int 17:1552-1561. doi:10.1007/s00198-006-0165-3

44. Mark H, Nilsson A, Nannmarl U, Rydevik B (2004) Effects of fracture fixation stability on ossification in healing fractures. Clin Orthop Relat Res. doi:10.1097/01.blo.0000116307.96693.b5

45. Xing Z, Lu C, Hu D, Yu YY, Wang X, Colnot C, Nakamura M, Wu Y, Miclau T, Marcucio RS (2010) Multiple roles for CCR2 during fracture healing. Dis Model Mech 3:451-458. doi:10.1242/dmm.003186

Figure legends

Fig. 1 Representative 3D images during fracture healing. The fracture gap in the fracture + SCI, BTX, and propranolol groups disappeared earlier than that of the fracture group did, and the bony union was observed earlier in these groups than that of the fracture group. The white arrowheads indicate the fracture gap

Fig. 2 The callus size of the fracture and fracture + SCI groups during fracture healing. The size of callus in the fracture + SCI group was significantly smaller than that of the fracture group at all the time points. *$p < 0.05$

Fig. 3 a Representative safranin-O-stained histological images of the fracture and fracture + SCI groups during fracture healing. The complete bridging of the fracture gap occurred earlier in the fracture + SCI group than that in the fracture group. Cb cortical bone, Ca cartilage tissue, Wb woven bone tissue. Scale bars 1 mm. **b** The temporal changes in the fibrous tissue area, cartilage tissue area, and newly formed bone area in the fracture callus of the fracture and fracture + SCI rats during fracture healing. At 7 days, the area of cartilage tissue in the fracture + SCI group was significantly smaller than that of the fracture group. *$p < 0.05$

Fig. 4 Representative safranin-O-stained histological images of the fracture, fracture + SCI, BTX, and propranolol groups at 14 and 28 days after fracture. The bony bridging of fracture gap in the BTX group occurred with immature woven bone, although no difference between the fracture + SCI and propranolol groups was observed. Cb cortical bone, Ca cartilage tissue, Wb woven bone tissue. Scale bars 1 mm

Fig. 5 Representative immunostaining images for type I, II, and X collagen of the fracture and fracture + SCI groups during fracture healing. At 7 days, the immunoreactivity of type I, II, and X collagen was observed in the callus of fractured rats. In contrast, the immunoreactivity of type I collagen was observed in the callus of fracture + SCI rats. At 14 days, the immunoreactivity of type I, II, and X collagen was observed in the callus of the fracture and fracture + SCI rats. The black arrows indicate immunoreactivity of type I collagen. The black arrowheads indicate the immunoreactivity of type II collagen. The white arrows indicate the immunoreactivity of type X collagen. Scale bar 500 μm

Fig. 6 Representative immunostaining images for CD68 of the fracture and fracture + SCI groups during fracture healing. The immunoreactivity of the fracture + SCI group

was lower than that of the fracture group. The black arrowheads indicate the immunoreactivity of CD68. Scale bar 1 mm

Supplemental Fig. 1 Study design with the assignment of animals to each group and the timeline of analyses.

Figure

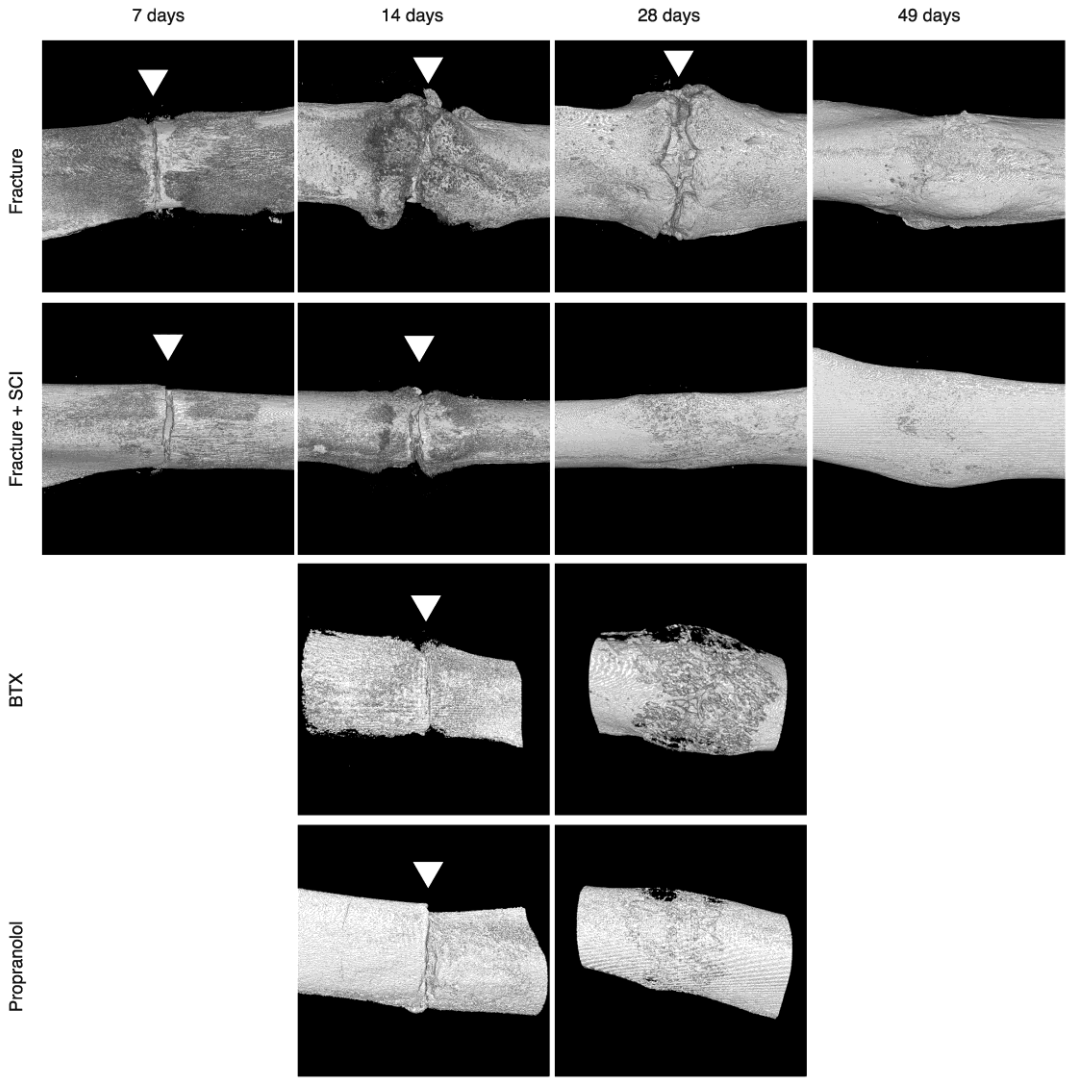
7 days
14 days
28 days
49 days
Fracture
Fracture + SCI
BTX
Propranolol

Fig. 1

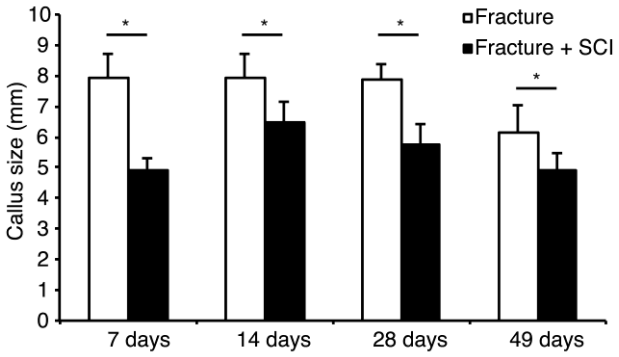
Callus size (mm)
10
9
8
7
6
5
4
3
2
1
0
*
*
*
*
Fracture
Fracture + SCI
7 days
14 days
28 days
49 days

Fig. 2

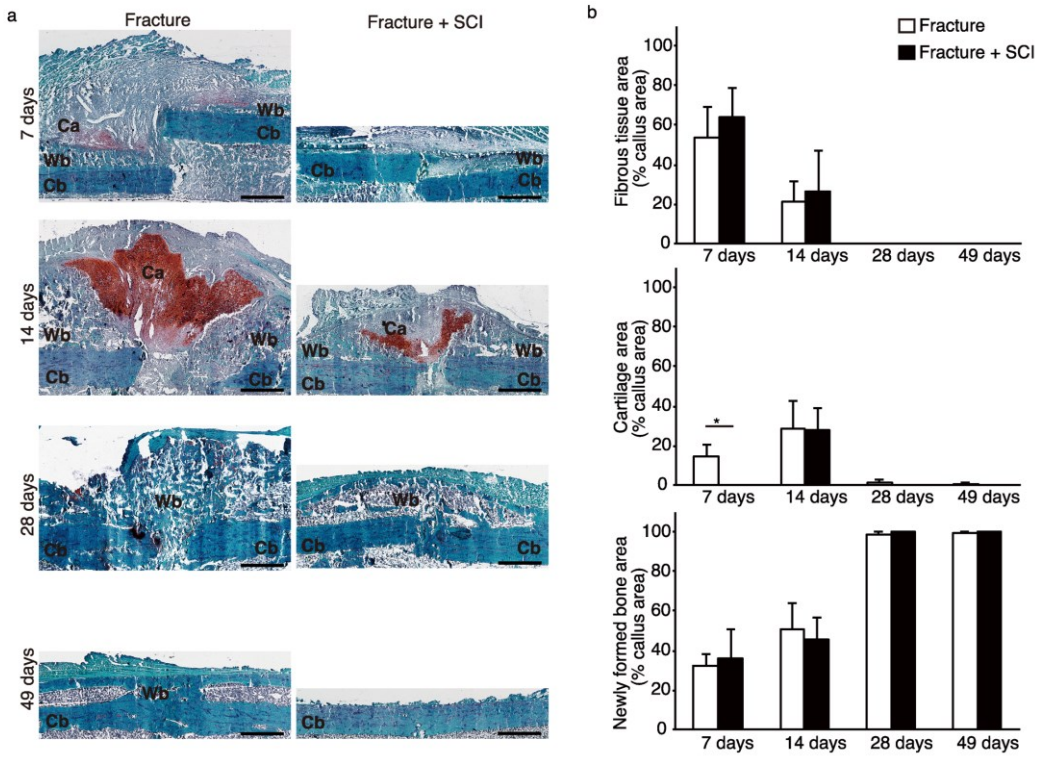
a
Fracture
Fracture + SCI
7 days
14 days
28 days
49 days
Ca
Wb
Cb
b
Fracture
Fracture + SCI
Fibrous tissue area (% callus area)
Cartilage area (% callus area)
Newly formed bone area (% callus area)
0
20
40
60
80
100
7 days
14 days
28 days
49 days
*

Fig. 3

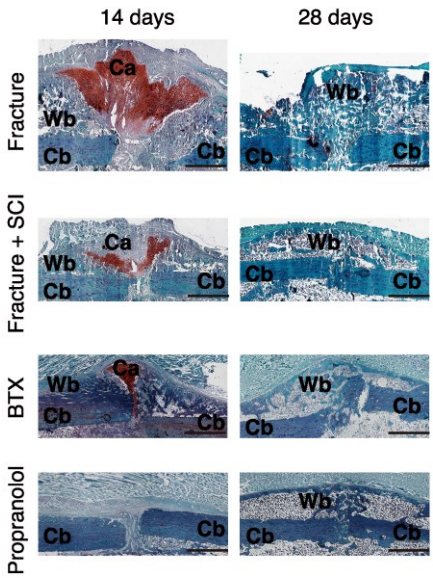
14 days
28 days
Fracture
Fracture + SCI
BTX
Propranolol
Ca
Wb
Cb

Fig. 4

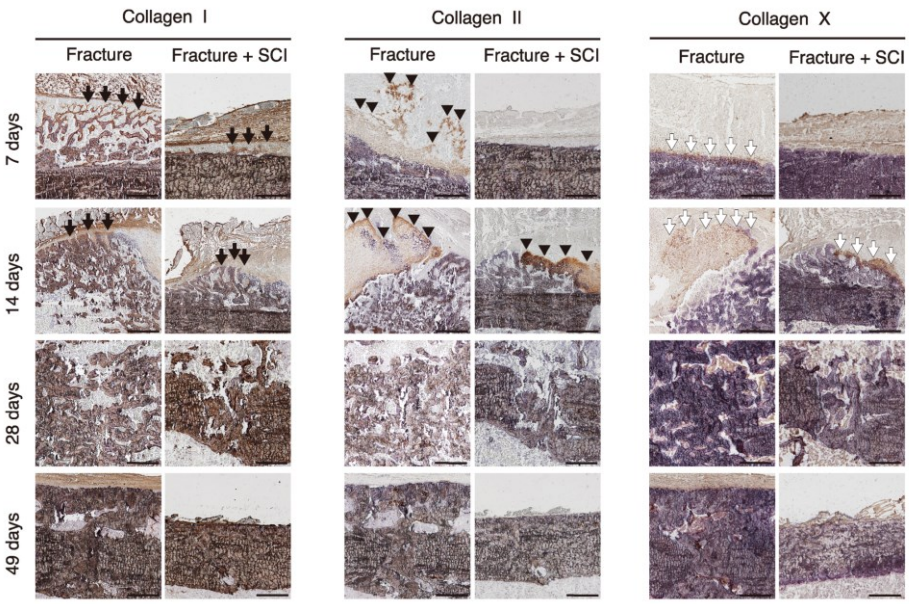
Collagen I
Collagen II
Collagen X
Fracture
Fracture + SCI
Fracture
Fracture + SCI
Fracture
Fracture + SCI
7 days
14 days
28 days
49 days

Fig. 5

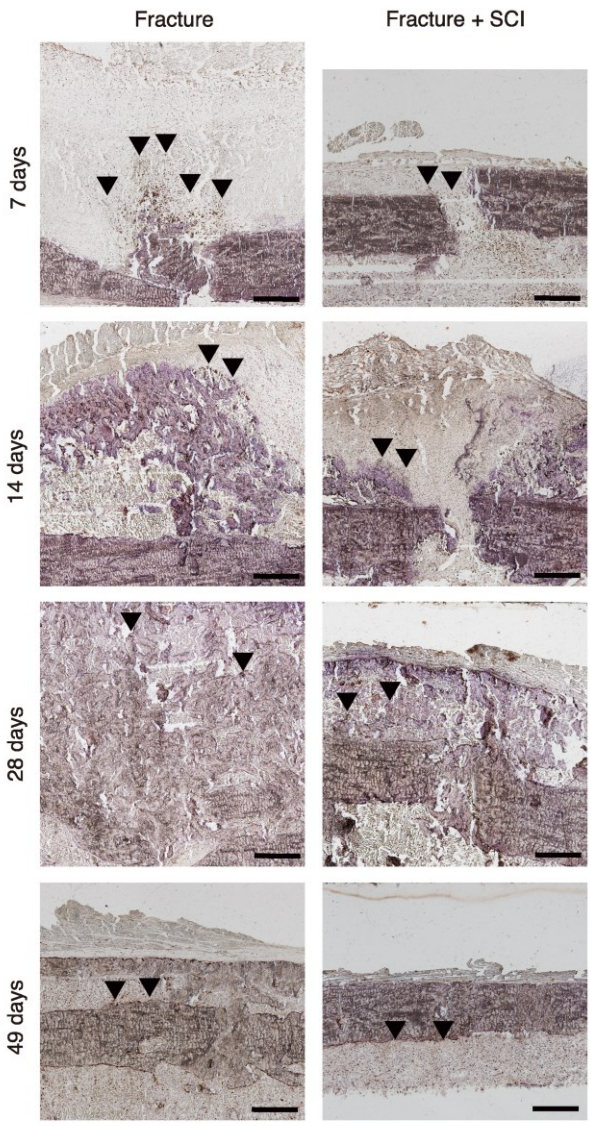

Fig. 6

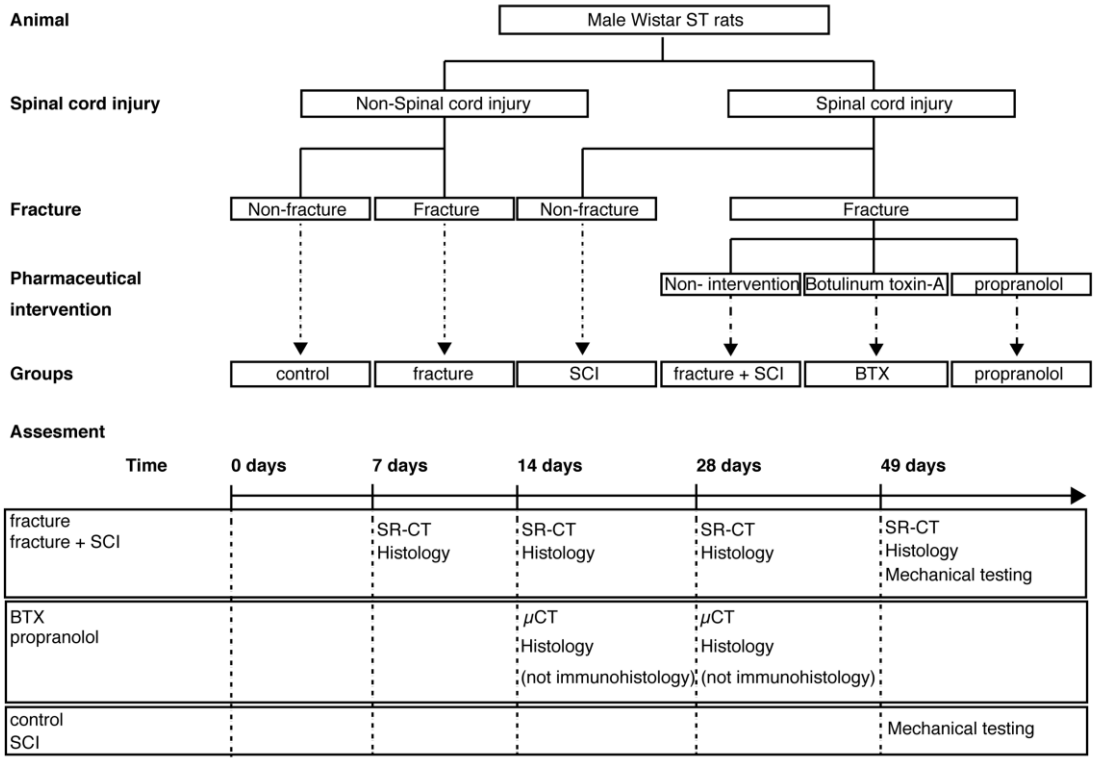

Supplemental Fig. 1